Threshold behaviour of optical frequency comb self-generation in an InAs/InGaAs quantum dot laser

Threshold behaviour of optical frequency comb self-generation in an InAs/InGaAs quantum dot laser

CHRISTOPH WEBER[1], LORENZO L. COLUMBO[2,*], MARIANGELA GIOANNINI[2], STEFAN BREUER[1], AND PAOLO BARDELLA[2]

[1] *Institute of Applied Physics, Technische Universität Darmstadt, Schlossgartenstraße 7, 64289 Darmstadt, Germany*
[2] *Dipartimento di Elettronica e Telecomunicazioni, Politecnico di Torino, Corso Duca degli Abruzzi 24, 10129 Torino, Italy*
[*] *Corresponding author: lorenzo.columbo@polito.it*

Compiled XXX

We report on a significant reduction of both the radio-frequency beat note line width at 40.7 GHz and the integrated relative intensity noise of a 1 mm long edge-emitting monolithic Fabry-Pérot InAs/InGaAs quantum dot semiconductor laser emitting from the ground state at 1250 nm by injection current control. For increasing injection currents, first an unlocked multi-mode behaviour is observed and then, at a certain current above lasing threshold, self-locking of the longitudinal modes due to internal non-linear effects occurs yielding a beat line width of 20 kHz (−3 dB) in contrast to tens of megahertz for lower injection currents. These results are confirmed by simulations.

OCIS codes: (140.5960) Semiconductor lasers, (230.5590) Quantum-well, -wire and -dot devices, (140.4050) Mode-locked lasers

http://dx.doi.org/10.1364/ao.XX.XXXXXX

Optical frequency combs (OFCs) generated by monolithic semiconductor lasers (SCLs) are ideal candidates for high-data rate optical interconnect systems based on silicon photonics [1], for the generation of sub-terahertz signals by comb line mixing on fast photo detectors [2, 3] and for dual-comb spectroscopy featuring high speed and good precision [4], as recently reported on the chip-scale level based on quantum cascade laser (QCL) [5]. OFCs offer a broad spectrum of frequency equidistant lasing modes with low phase noise, amplitude noise and nearly equally distributed spectral power [6]. Thereby, in monolithic SCLs, the longitudinal modes are phase-locked without the need for a saturable absorber or any active optical or electrical modulation. The underlying physical effects causing this self mode-locking (SML) are yet to be fully understood and are thus subject to intensive theoretical and experimental investigations, although a fundamental role is played by four-wave-mixing (FWM) [7–14]. Recently, by applying a time-domain traveling-wave (TDTW) model, the multi-longitudinal mode dynamics of a 250 µm long single-section SML quantum dot (QD) laser has been simulated including the sub-wavelength carrier grating that is not washed out by diffusion in zero-dimension QDs. The numerical results showed that multi-mode emission can be observed directly at the lasing threshold, and that by increasing the injected gain current, a transition from unlocked regime to SML due to FWM occurs in the simulations [13].

Experimentally, SML has been reported for single-section Fabry-Pérot quantum well (QW) SCL [15–17], quantum dash (QDash) SCL [18–20], QCL SCL [4, 5, 12, 21] and QD SCL [22, 23]. The first integrated single-section SML laser on a CMOS compatible Si-platform has been demonstrated recently [24]. Ultrashort pulses of 312 fs directly at the laser output facet have been reported [23], or dispersion compensation by a single mode fiber is employed to access pulses as short as 600 fs [20]. Single-section SCLs with low-dimensional active regions have been used to generate OFCs at near-infrared wavelengths with −3 dB optical comb-widths of up to 15 nm [7] and up to 110 optical modes [9]. OFCs with a mode-spacing of 4.4 GHz, corresponding to a 10 mm long SCL laser [9], and up to 100 GHz in a 0.24 mm long device [10] have been realized. While SML in some devices is reported to start directly at the lasing threshold and is observed for all currents [23], others exhibit regimes of SML or irregular behavior corresponding to narrow and large radio frequency (RF) line widths respectively [25] as can be derived from simulations (see, e.g., [13]). The RF beat note line width was used in QCLs to characterize different operation regimes depending on injected current and operating temperature [21]; narrow beat note values indicate OFC.

Here, we investigate the RF line width and the integrated relative intensity noise (RIN) characteristics of a single-section QD SCL. In particular, we find experimentally that well above lasing threshold at a certain value of the gain current, multi-mode emission of the laser switches from uncorrelated modes to SML. In fact, an RF line width reduction from tens of megahertz to tens of kilohertz is accompanied with a substantial reduction of the integrated RIN. The theoretical predictions are in very good agreement with the experimental data.

Experimentally, a single-section Fabry-Pérot ridge waveguide QD SCL is studied. The active region consists of 10 layers of InAs/InGaAs QDs. The facets are as-cleaved and the ridge is 6 µm wide. The laser length of 1 mm corresponds to an optical mode spacing (RF beat note frequency) of 40.7 GHz. The laser cooling block temperature is stabilized to 10 °C. Gain currents up to 400 mA are injected into the laser corresponding to a maxi-

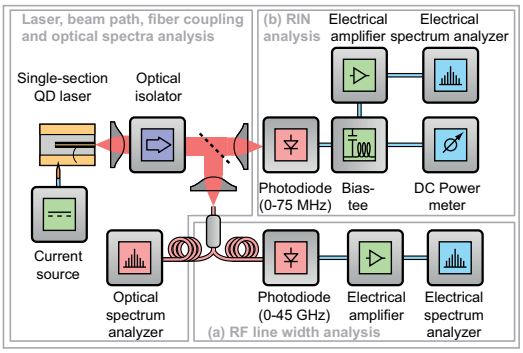

Fig. 1. Schematic experimental setups for (a) RF line width and (b) RIN measurements.

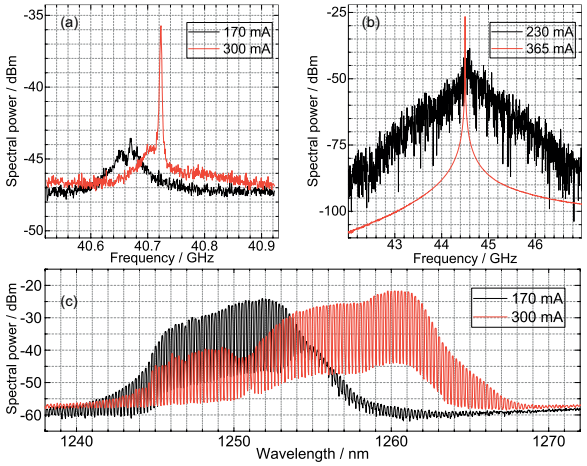

Fig. 2. Exemplary (a) experimentally obtained and (b) simulated RF beat note spectra for a current below (black) and a current above (red) the mode-locked (ML) threshold. (c) Experimental optical spectra for corresponding currents.

mum current density of 6.6 kA cm^{-1}. The laser emission wavelength is centered around 1250 nm and the lasing threshold at this temperature amounts to 16 mA. The developed and adapted experimental setups for RF line width and integrated RIN measurement [26] and analysis are depicted schematically in Fig. 1. To measure and analyze the RF beat note, the emitted light from the laser is coupled into a standard single-mode optical fiber and is detected by a fast photo diode connected to an amplifier and an electrical spectrum analyzer (ESA) (bandwidth 50 GHz). An optical isolator before the fiber coupling (isolation $>$ 60 dB) prevents unwanted optical feedback. The RF beat note line width is determined by well-matching Lorentzian fits to the RF beat note and is directly related to the pulse-to-pulse timing jitter SCL [27, 28]. The optical spectra are obtained using an optical spectrum analyzer (OSA) (spectral resolution 0.01 nm). The integrated RIN of all modes is measured by splitting the signal of a free-space photo diode into an AC and a DC part by a bias-tee. The amplified AC part is integrated using a 1.5 GHz ESA while the DC part is detected by a multi-meter. This direct detection technique has been validated in previous works [26, 29]. We focus on the low frequency fluctuations (10 MHz to 50 MHz) of the RIN, since this is the interval where we expect to observe a significant difference between the locked and unlocked configurations [13]. Two RF beat note spectra experimentally acquired for 170 mA and 300 mA are depicted in Fig. 2a where −3 dB widths of 144 MHz and 2.75 MHz are found by Lorentzian fits to a zoom into the beat notes. We attribute the broad beat note centered at 40.67 GHz to emission of unlocked longitudinal modes whereas the narrow one centered at 40.72 GHz indicates locked longitudinal modes in agreement for e.g. with the theoretical results reported in [13]. The corresponding optical spectra are depicted in Fig. 2c. For certain currents, we observe a second RF beat note with significantly lower spectral peak power than the central RF beat note. It can be attributed to the appearance of a second group of longitudinal modes in the optical spectra. The broad RF beat note line widths of two- or three-digit megahertz indicate that these modes are not locked. Such a splitting of the optical spectrum has also been described in [30]. By systematically increasing the gain current up to 400 mA in steps of 5 mA and fitting Lorentzian curves to the main beat notes, the beat note frequencies and corresponding −3 dB RF line widths are studied experimentally. The beat note frequency shifts to higher frequencies with higher injection currents by 0.125 MHz/mA. The recorded RF line widths are depicted in Fig. 3a as a function of gain current. Up to a gain current of 190 mA, line widths from 9 MHz to 50 MHz are evident. Above this threshold denoted by a dashed red line in Fig. 3, the RF line width reduces significantly to a minimum of 20 kHz at 230 mA. The inset of Fig. 3a depicts RF beat note line width for a selected current range on a logarithmic scale. The measured integrated RIN of all modes is depicted in Fig. 3b in dependence on the gain current up to 250 mA. The current has been increased in steps of 5 mA. The integrated RIN values are decreasing with increasing current with a steepest decrease of 0.36 (dBc/Hz)/mA for currents ranging from 170 mA up to the SML threshold of 190 mA. The minimum RIN amounts to −148 dBc/Hz and is identified well above the SML threshold. Experimentally, the particular integrated RIN characteristics and RF trends indicate the existence of two regimes, one with unlocked multi-modal emission and a second with locking or SML of the longitudinal modes. A distinct current threshold appears to exist between both regimes.

In order to theoretically reproduce these experimental results, we describe the coherent interaction between QDs inhomogeneous broadened gain medium and the intracavity electric field trough a set of coupled traveling wave equations for the slowly varying envelope of the fundamental TE electric field $E^{\pm}(z,t)$ and of the slowly varying envelope of the microscopic polarizations $p_i^{\pm}(z,t)$, coupled with the evolution equations for the electron occupation probabilities of ground state ρ_i in each dot sub-group i and in the wetting layer (WL) ρ_{WL} [31, 32]. The standing wave pattern due to the interference between forward and backward fields generates a grating in the carrier density that is not washed out by diffusion in zero dimension active media such as QDs. This effect is taken into account by deriving the evolution equations for the first Fourier components of the spatial grating denoted as ρ_i^+ and ρ_{WL}^+ following the procedure highlighted in [13]. Thereby, the cavity length can be discretized in spatial steps of few microns, but still the effects of a fast standing wave pattern on the carrier dynamics can be investigated [33–36]. The resulting multi-populations TDTW model is a more accurate version of the one recently used by the authors [13] since it accounts for the medium polarizations dynamics beyond any adiabatic approximation and it includes the inhomogeneous broadening of the gain line width associated with the normal distributions of the self-assembled QD sizes.

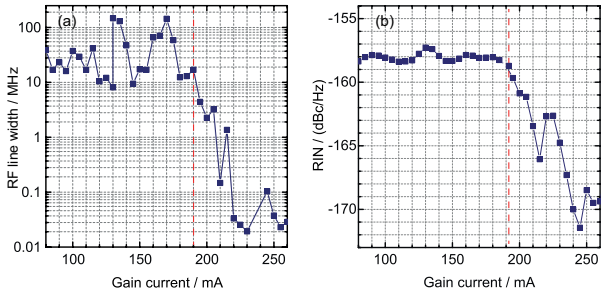

Fig. 3. Experimental results for a 1 mm long QD laser. (a) RF line widths (b) integrated RIN (10 MHz to 50 MHz) versus gain current. Dashed red lines: transition to SML.

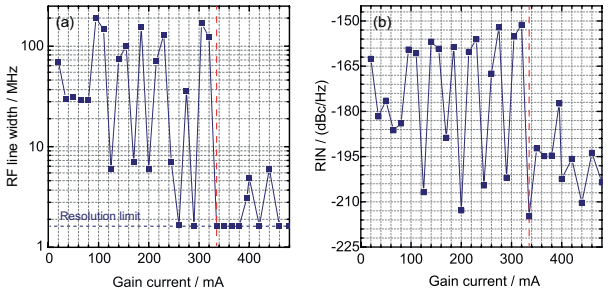

Fig. 4. Simulation results for a 1 mm long QD laser. (a) RF line widths and (b) integrated RIN (from 10 MHz to 50 MHz) versus gain current. Dashed red lines: transition to SML.

The new set of TDTW dynamical equations reads:

$$\frac{\partial E^{\pm}(z,t)}{\partial t} = \gamma_p\left(\mp\frac{\partial E^{\pm}}{\partial z} - \frac{\alpha_{wg}L}{2}E^{\pm} - C\sum_{i=-N}^{N}\bar{G}_i p_i^{\pm} + S_{sp}^{\pm}\right) \quad (1)$$

$$\frac{\partial p_i^{\pm}(z,t)}{\partial t} = (j\delta_i/\Gamma - 1)p_i^{\pm} - D\left[(2\rho_i - 1)E^{\pm} + 2\rho_i^{\pm}E^{\mp}\right] \quad (2)$$

$$\frac{\partial \rho_i(z,t)}{\partial t} = -\gamma_e\rho_i(1-\rho_{0,WL}) + F\gamma_C\rho_{WL}(1-\rho_i) - \gamma_{sp}\rho_i^2 - \gamma_{nr}^{GS}\rho_i + H\,Re\left(E^{+*}p_i^{+} + E^{-*}p_i^{-}\right) \quad (3)$$

$$\frac{\partial \rho_i^{+}(z,t)}{\partial t} = -\gamma_e\rho_i^{+}(1-\rho_{WL}) + \gamma_e\rho_i\rho_{WL}^{+} - F\gamma_C\rho_{WL}\rho_i^{+} + F\gamma_C\rho_{WL}^{+}(1-\rho_i) - \gamma_{sp}\rho_i\rho_i^{+} - \gamma_{nr}^{GS}\rho_i^{+} + \frac{H\,d*}{4}\left(\frac{E^{+}p_i^{-*}}{d} + \frac{E^{-*}p_i^{+}}{d^*}\right) \quad (4)$$

$$\frac{\partial \rho_{WL}(z,t)}{\partial t} = \sum_{i=-N}^{N}\left[-\bar{G}_i\gamma_C\rho_{WL}(1-\rho_i) + \frac{\bar{G}_i}{F}\gamma_e\rho_i(1-\rho_{WL})\right] + \Lambda\tau_d - \gamma_{nr}^{WL}\rho_{WL} \quad (5)$$

$$\frac{\partial \rho_{WL}^{+}(z,t)}{\partial t} = \sum_{i=-N}^{N}\left[\frac{\bar{G}_i}{F}\gamma_e\rho_i^{+}(1-\rho_{WL}) - \bar{G}_i\gamma_C\rho_{WL}^{+}(1-\rho_i) - \frac{\bar{G}_i}{F}\gamma_e\rho_i\rho_{WL}^{+} + \bar{G}_i\gamma_C\rho_{WL}\rho_i^{+}\right] - \gamma_{nr}^{WL}\rho_{WL}^{+} \quad (6)$$

In the compact adimensional formulation provided by Eqs. (1)–(6) we scaled time to the fastest time scale in the system represented by the dipole dephasing time τ_d and the longitudinal coordinate to the cavity length L and the complex dynamical variables $E^{\pm}$ and $p_i^{\pm}$ are normalized as in [13]; α_{wg} represents the waveguide losses, $\gamma_p = \tau_d v_g/L$ is the normalized photon decay rate, $\gamma_{e,C} = \tau_d/\tau_{e,C}$ are the normalized escape and capture rates, $\gamma_{sp} = \tau_d/\tau_{sp}$ is the normalized spontaneous decay rate from the ground state, $\gamma_{nr}^{WL,GS} = \tau_d/\tau_{nr}^{WL,GS}$ represents the normalized nonradiative decay rates and Λ is the carriers injection probability per unit time. Finally, $\bar{G}_i$ is the probability that a QD belongs to the sub-group i and it follows a Gaussian distribution. The adimensional parameters C, D, F, H have the following expressions:

$$C = \frac{\omega_0 L\Gamma_{xy}\mu}{2c\eta},\ D = \frac{d^2 N_D}{\epsilon_0\hbar\Gamma h_{QD}},\ F = \frac{D_{WL}}{\mu N_D},\ H = \frac{\tau_{sp}\Gamma^2\omega_0\Gamma_{xy}\hbar\epsilon_0 h_{QD}}{\eta\omega_i d^2 N_D}$$

where ω_0 is our reference angular frequency coincident with the cold cavity mode closest to the ground state gain peak, Γ_{xy} is the transverse optical confinement factor in the total QD active region, μ is the degeneracy of the ground state, η is the effective refractive index, d is the dipole matrix element associated with the optical transition from ground level, N_D is the number of QDs per unit area, $\Gamma = 1/\tau_d$, h_{QD} is the QDs layer thickness, D_{WL} is the number of WL level per unit area per QDs layer, and ω_i is the frequency of transition from the ground state of the i group so that $\delta_i = \omega_i - \omega_0$, In Eq. (1) we take into account the spontaneous emission trough the terms $S_{sp}^{\pm}$, which have the same expression introduced in [37]. In the Fabry-Pérot edge emitting configuration, the field envelopes satisfy the boundary conditions $E^{+}(0,t) = r_1E^{-}(0,t)$ and $E^{-}(L,t) = r_2E^{+}(L,t)$, with $r_{1,2}$ reflection coefficients at the two SCL facets. The system of coupled Eq.s (1)–(6) is numerically solved using a Finite Difference discretization scheme integrated in time using a 2nd order Runge-Kutta method. For this study we considered a 30 fs integration time step. For our simulations, we use the same values of the material and device parameters introduced in [32], except for the device length which is chosen as in the experiment (L =1 mm) and the full-width at half maximum of the inhomogeneous broadening, set to 2.4 THz (and corresponding to three QD populations) to better reproduce the experimentally estimated SML threshold.

In the simulations, two regimes are observed when increasing the gain current, which is in qualitative agreement with the experiments. Right above the lasing threshold, multi-modal emission is identified whereas these mode have no constant phase difference. By further increasing the gain current, a sharp transition to a regime of locked laser modes is evident. In this regime, adjacent modes in the optical spectrum have a constant phase relation, but the phase difference between adjacent modes deviates across the whole spectrum [13]. Therefore, in the simulation, optical pulses cannot be observed directly at the laser output. In Fig. 2b two exemplary simulated RF spectra are depicted. The black colored spectrum corresponds to a low gain current of 230 mA and thus the laser operates in the unlocked regime. The red colored spectrum is simulated for an injected gain current of 365 mA, where the modes are locked. In the regime of SML operation a significant reduction in the RF line width is evident. In Fig. 4a, the −3 dB line width of the simulated RF beat note spectra is plotted in dependence on the injected gain current. Again, in agreement with the experimental outcomes, as a general trend, a significant narrowing of the beat note above the locking threshold is observed, indicated by the red dashed line, from hundreds of megahertz to few megahertz, that represents the resolution limit of our numerical analysis. The locking threshold strongly depends on the self-injection locking mechanism [38], caused by FWM, which depends in turn on the physical and geometrical

device parameters. This might explain the difference between the locking thresholds currents of the experimental and numerical results reported here. In Fig. 4b the simulated integrated RIN is depicted as a function of gain current. The lowest RIN values are found above the locking threshold, while a steplike transition occurs at that threshold. Numerical simulations also suggest a reduction of the optical line width and the RIN of the single longitudinal modes, as discussed in [13], which will be a subject of future experimental investigations. In agreement with the results presented in Fig. 3 and with other experimental findings about SML in low-dimensional SCLs [39], we observe current intervals where an alternance between broad and narrow RF beat notes may exist. Although, the origin of this peculiar phenomenon, that it likely to involve complex nonlinear processes in radiation-semiconductor interaction, is not fully understood yet, a tentative interpretation based on phase-transition theory is outlined in [13].

In this contribution, the self-locking of longitudinal modes in a 1 mm long single-section QD SCL emitting from the ground state centered at 1250 nm is investigated, with experiments and by TDTW simulations, studying the RF beat note line width and integrated RIN. A SML threshold well above the actual lasing threshold is observed. Experimentally, this locking threshold is characterized by a reduction of the RF beat note line width to 20 kHz and the integrated RIN. This novel threshold behavior is confirmed by the numerical simulations.

FUNDING

German Research Foundation (38919332).

ACKNOWLEDGEMENTS

The authors thank W. Elsäßer for support, W. Rök for technical assistance and two anonymous reviewers for their constructive criticism.

REFERENCES

1. P. Delfyett, S. Gee, M.-T. Choi, H. Izadpanah, W. Lee, S. Ozharar, F. Quinlan, and T. Yilmaz, Journal of Lightwave Technology **24**, 2701 (2006).
2. S. Koenig, D. Lopez-Diaz, J. Antes, F. Boes, R. Henneberger, A. Leuther, A. Tessmann, R. Schmogrow, D. Hillerkuss, R. Palmer, T. Zwick, C. Koos, W. Freude, O. Ambacher, J. Leuthold, and I. Kallfass, Nature Photonics **7**, 977 (2013).
3. S. Latkowski, F. Surre, and P. Landais, Applied Physics Letters **92**, 081109 (2008).
4. J. Faist, G. Villares, G. Scalari, M. Rösch, C. Bonzon, A. Hugi, and M. Beck, Nanophotonics **5** (2016).
5. J. Hillbrand, A. M. Andrews, H. Detz, G. Strasser, and B. Schwarz, Nature Photonics (2018).
6. A. Schliesser, N. Picqué, and T. W. Hänsch, Nature Photonics **6**, 440 (2012).
7. R. Rosales, K. Merghem, A. Martinez, A. Akrout, J.-P. Tourrenc, A. Accard, F. Lelarge, and A. Ramdane, IEEE Journal of Selected Topics in Quantum Electronics **17**, 1292 (2011).
8. F. Lelarge, B. Dagens, J. Renaudier, R. Brenot, A. Accard, F. van Dijk, D. Make, O. L. Gouezigou, J.-G. Provost, F. Poingt, J. Landreau, O. Drisse, E. Derouin, B. Rousseau, F. Pommereau, and G.-H. Duan, IEEE Journal of Selected Topics in Quantum Electronics **13**, 111 (2007).
9. M. Faugeron, F. Lelarge, M. Tran, Y. Robert, E. Vinet, A. Enard, J. Jacquet, and F. V. Dijk, IEEE Journal of Selected Topics in Quantum Electronics **19**, 1101008 (2013).
10. A. Akrout, A. Shen, R. Brenot, F. V. Dijk, O. Legouezigou, F. Pommereau, F. Lelarge, A. Ramdane, and G.-H. Duan, IEEE Photonics Technology Letters **21**, 1746 (2009).
11. C. Gosset, K. Merghem, A. Martinez, G. Moreau, G. Patriarche, G. Aubin, A. Ramdane, J. Landreau, and F. Lelarge, Applied Physics Letters **88**, 241105 (2006).
12. A. Hugi, G. Villares, S. Blaser, H. C. Liu, and J. Faist, Nature **492**, 229 (2012).
13. P. Bardella, L. L. Columbo, and M. Gioannini, Optics Express **25**, 26234 (2017).
14. M. Piccardo, D. Kazakov, B. Schwarz, P. Chevalier, A. Amirzhan, J. Hillbrand, S. Z. AlMutairi, Y. Wang, F. Xie, K. Lascola, S. Becker, L. Hildebrandt, R. Weih, A. Belyanin, and F. Capasso, IEEE Journal of Selected Topics in Quantum Electronics **25**, 1 (2019).
15. K. Sato, Electronics Letters **37**, 763 (2001).
16. R. Maldonado-Basilio, S. Latkowski, F. Surre, and P. Landais, Optics Communications **283**, 299 (2010).
17. C. Calò, V. Vujicic, R. Watts, C. Browning, K. Merghem, V. Panapakkam, F. Lelarge, A. Martinez, B.-E. Benkelfat, A. Ramdane, and L. P. Barry, Optics Express **23**, 26442 (2015).
18. S. Latkowski, R. Maldonado-Basilio, and P. Landais, Opt. Express **17**, 19166 (2009).
19. V. Panapakkam, A. P. Anthur, V. Vujicic, R. Zhou, Q. Gaimard, K. Merghem, G. Aubin, F. Lelarge, E. A. Viktorov, L. P. Barry, and A. Ramdane, IEEE Journal of Quantum Electronics **52**, 1 (2016).
20. R. Rosales, S. G. Murdoch, R. Watts, K. Merghem, A. Martinez, F. Lelarge, A. Accard, L. P. Barry, and A. Ramdane, Optics Express **20**, 8649 (2012).
21. M. Wienold, B. Roben, L. Schrottke, and H. T. Grahn, Optics Express **22**, 30410 (2014).
22. J. Liu, Z. Lu, S. Raymond, P. J. Poole, P. J. Barrios, and D. Poitras, Optics Letters **33**, 1702 (2008).
23. Z. G. Lu, J. R. Liu, S. Raymond, P. J. Poole, P. J. Barrios, and D. Poitras, Optics Express **16**, 10835 (2008).
24. S. Liu, D. Jung, J. C. Norman, M. J. Kennedy, A. C. Gossard, and J. E. Bowers, Electronics Letters **54**, 432 (2018).
25. J. Müller, J. Hauck, B. Shen, S. Romero-García, E. Islamova, S. S. Azadeh, S. Joshi, N. Chimot, A. Moscoso-Mártir, F. Merget, F. Lelarge, and J. Witzens, Advanced Optical Technologies **4**, 119 (2015).
26. R. Pawlus, L. L. Columbo, P. Bardella, S. Breuer, and M. Gioannini, Optics Letters **43**, 867 (2018).
27. F. Kefelian, S. O'Donoghue, M. T. Todaro, J. G. McInerney, and G. Huyet, IEEE Photonics Technology Letters **20**, 1405 (2008).
28. L. Drzewietzki, S. Breuer, and W. Elsäßer, Opt. Express **21**, 16142 (2013).
29. R. Pawlus, S. Breuer, and M. Virte, Optics Letters **42**, 4259 (2017).
30. E. A. Viktorov, T. Habruseva, S. P. Hegarty, G. Huyet, and B. Kelleher, Physical Review Letters **112**, 224101 (2014).
31. M. Gioannini, P. Bardella, and I. Montrosset, IEEE Journal of Selected Topics in Quantum Electronics **21**, 698 (2015).
32. L. L. Columbo, P. Bardella, and M. Gioannini, Opt. Express **26**, 19044 (2018).
33. M. Homar, J. V. Moloney, and M. S. Miguel, IEEE Journal of Quantum Electronics **32**, 553 (1996).
34. A. Gordon, C. Y. Wang, L. Diehl, F. X. Kärtner, A. Belyanin, D. Bour, S. Corzine, G. Höfler, H. C. Liu, H. Schneider, T. Maier, M. Troccoli, J. Faist, and F. Capasso, Physical Review A **77**, 053804 (2008).
35. J. Javaloyes and S. Balle, IEEE Journal of Quantum Electronics **46**, 1023 (2010).
36. A. Pérez-Serrano, J. Javaloyes, and S. Balle, Optics Express **19**, 3284 (2011).
37. M. Rossetti, P. Bardella, and I. Montrosset, IEEE Journal of Quantum Electronics **47**, 139 (2011).
38. J. Renaudier, G.-H. Duan, P. Landais, and P. Gallion, IEEE Journal of Quantum Electronics **43**, 147 (2007).
39. J. Müller, J. Hauck, B. Shen, S. Romero-García, E. Islamova, S. S. Azadeh, S. Joshi, N. Chimot, A. Moscoso-Mártir, F. Merget, F. Lelarge, and J. Witzens, Advanced Optical Technologies **4** (2015).

FULL REFERENCES

1. P. Delfyett, S. Gee, M.-T. Choi, H. Izadpanah, W. Lee, S. Ozharar, F. Quinlan, and T. Yilmaz, "Optical frequency combs from semiconductor lasers and applications in ultrawideband signal processing and communications," Journal of Lightwave Technology **24**, 2701–2719 (2006).
2. S. Koenig, D. Lopez-Diaz, J. Antes, F. Boes, R. Henneberger, A. Leuther, A. Tessmann, R. Schmogrow, D. Hillerkuss, R. Palmer, T. Zwick, C. Koos, W. Freude, O. Ambacher, J. Leuthold, and I. Kallfass, "Wireless sub-THz communication system with high data rate," Nature Photonics **7**, 977–981 (2013).
3. S. Latkowski, F. Surre, and P. Landais, "Terahertz wave generation from a dc-biased multimode laser," Applied Physics Letters **92**, 081109 (2008).
4. J. Faist, G. Villares, G. Scalari, M. Rösch, C. Bonzon, A. Hugi, and M. Beck, "Quantum cascade laser frequency combs," Nanophotonics **5** (2016).
5. J. Hillbrand, A. M. Andrews, H. Detz, G. Strasser, and B. Schwarz, "Coherent injection locking of quantum cascade laser frequency combs," Nature Photonics (2018).
6. A. Schliesser, N. Picqué, and T. W. Hänsch, "Mid-infrared frequency combs," Nature Photonics **6**, 440–449 (2012).
7. R. Rosales, K. Merghem, A. Martinez, A. Akrout, J.-P. Tourrenc, A. Accard, F. Lelarge, and A. Ramdane, "InAs/InP quantum-dot passively mode-locked lasers for 1.55-μ m applications," IEEE Journal of Selected Topics in Quantum Electronics **17**, 1292–1301 (2011).
8. F. Lelarge, B. Dagens, J. Renaudier, R. Brenot, A. Accard, F. van Dijk, D. Make, O. L. Gouezigou, J.-G. Provost, F. Poingt, J. Landreau, O. Drisse, E. Derouin, B. Rousseau, F. Pommereau, and G.-H. Duan, "Recent advances on InAs/InP quantum dash based semiconductor lasers and optical amplifiers operating at 1.55 μm," IEEE Journal of Selected Topics in Quantum Electronics **13**, 111–124 (2007).
9. M. Faugeron, F. Lelarge, M. Tran, Y. Robert, E. Vinet, A. Enard, J. Jacquet, and F. V. Dijk, "High peak power, narrow RF linewidth asymmetrical cladding quantum-dash mode-locked lasers," IEEE Journal of Selected Topics in Quantum Electronics **19**, 1101008–1101008 (2013).
10. A. Akrout, A. Shen, R. Brenot, F. V. Dijk, O. Legouezigou, F. Pommereau, F. Lelarge, A. Ramdane, and G.-H. Duan, "Separate error-free transmission of eight channels at 10 gb/s using comb generation in a quantum-dash-based mode-locked laser," IEEE Photonics Technology Letters **21**, 1746–1748 (2009).
11. C. Gosset, K. Merghem, A. Martinez, G. Moreau, G. Patriarche, G. Aubin, A. Ramdane, J. Landreau, and F. Lelarge, "Subpicosecond pulse generation at 134ghz using a quantum-dash-based fabry-perot laser emitting at 1.56μm," Applied Physics Letters **88**, 241105 (2006).
12. A. Hugi, G. Villares, S. Blaser, H. C. Liu, and J. Faist, "Mid-infrared frequency comb based on a quantum cascade laser," Nature **492**, 229–233 (2012).
13. P. Bardella, L. L. Columbo, and M. Gioannini, "Self-generation of optical frequency comb in single section quantum dot fabry-perot lasers: a theoretical study," Optics Express **25**, 26234 (2017).
14. M. Piccardo, D. Kazakov, B. Schwarz, P. Chevalier, A. Amirzhan, J. Hillbrand, S. Z. AlMutairi, Y. Wang, F. Xie, K. Lascola, S. Becker, L. Hildebrandt, R. Weih, A. Belyanin, and F. Capasso, "Light and microwaves in laser frequency combs: An interplay of spatiotemporal phenomena," IEEE Journal of Selected Topics in Quantum Electronics **25**, 1–12 (2019).
15. K. Sato, "100 GHz optical pulse generation using fabry-perot laser under continuous wave operation," Electronics Letters **37**, 763 (2001).
16. R. Maldonado-Basilio, S. Latkowski, F. Surre, and P. Landais, "Linewidth analysis of 40-ghz passively mode-locked multi-mode semiconductor lasers," Optics Communications **283**, 299 – 303 (2010).
17. C. Calò, V. Vujicic, R. Watts, C. Browning, K. Merghem, V. Panapakkam, F. Lelarge, A. Martinez, B.-E. Benkelfat, A. Ramdane, and L. P. Barry, "Single-section quantum well mode-locked laser for 400 Gb/s SSB-OFDM transmission," Optics Express **23**, 26442 (2015).
18. S. Latkowski, R. Maldonado-Basilio, and P. Landais, "Sub-picosecond pulse generation by 40-ghz passively mode-locked quantum-dash 1-mm-long fabry-pérot laser diode," Opt. Express **17**, 19166–19172 (2009).
19. V. Panapakkam, A. P. Anthur, V. Vujicic, R. Zhou, Q. Gaimard, K. Merghem, G. Aubin, F. Lelarge, E. A. Viktorov, L. P. Barry, and A. Ramdane, "Amplitude and phase noise of frequency combs generated by single-section InAs/InP quantum-dash-based passively and actively mode-locked lasers," IEEE Journal of Quantum Electronics **52**, 1–7 (2016).
20. R. Rosales, S. G. Murdoch, R. Watts, K. Merghem, A. Martinez, F. Lelarge, A. Accard, L. P. Barry, and A. Ramdane, "High performance mode locking characteristics of single section quantum dash lasers," Optics Express **20**, 8649 (2012).
21. M. Wienold, B. Roben, L. Schrottke, and H. T. Grahn, "Evidence for frequency comb emission from a fabry-pérot terahertz quantum-cascade laser," Optics Express **22**, 30410–30424 (2014).
22. J. Liu, Z. Lu, S. Raymond, P. J. Poole, P. J. Barrios, and D. Poitras, "Dual-wavelength 925 GHz self-mode-locked InP-based quantum dot laser," Optics Letters **33**, 1702 (2008).
23. Z. G. Lu, J. R. Liu, S. Raymond, P. J. Poole, P. J. Barrios, and D. Poitras, "312-fs pulse generation from a passive c-band InAs/InP quantum dot mode-locked laser," Optics Express **16**, 10835 (2008).
24. S. Liu, D. Jung, J. C. Norman, M. J. Kennedy, A. C. Gossard, and J. E. Bowers, "490 fs pulse generation from passively mode-locked single section quantum dot laser directly grown on on-axis gap/si," Electronics Letters **54**, 432–433 (2018).
25. J. Müller, J. Hauck, B. Shen, S. Romero-García, E. Islamova, S. S. Azadeh, S. Joshi, N. Chimot, A. Moscoso-Mártir, F. Merget, F. Lelarge, and J. Witzens, "Silicon photonics WDM transmitter with single section semiconductor mode-locked laser," Advanced Optical Technologies **4**, 119–145 (2015).
26. R. Pawlus, L. L. Columbo, P. Bardella, S. Breuer, and M. Gioannini, "Intensity noise behavior of an inas/ingaas quantum dot laser emitting on ground states and excited states," Optics Letters **43**, 867–870 (2018).
27. F. Kefelian, S. O'Donoghue, M. T. Todaro, J. G. McInerney, and G. Huyet, "RF linewidth in monolithic passively mode-locked semiconductor laser," IEEE Photonics Technology Letters **20**, 1405–1407 (2008).
28. L. Drzewietzki, S. Breuer, and W. Elsäßer, "Timing jitter reduction of passively mode-locked semiconductor lasers by self- and external-injection: Numerical description and experiments," Opt. Express **21**, 16142–16161 (2013).
29. R. Pawlus, S. Breuer, and M. Virte, "Relative intensity noise reduction in a dual-state quantum-dot laser by optical feedback," Optics Letters **42**, 4259–4262 (2017).
30. E. A. Viktorov, T. Habruseva, S. P. Hegarty, G. Huyet, and B. Kelleher, "Coherence and incoherence in an optical comb," Physical Review Letters **112**, 224101 (2014).
31. M. Gioannini, P. Bardella, and I. Montrosset, "Time-domain traveling-wave analysis of the multimode dynamics of quantum dot fabry-perot lasers," IEEE Journal of Selected Topics in Quantum Electronics **21**, 698–708 (2015).
32. L. L. Columbo, P. Bardella, and M. Gioannini, "Self-pulsing in single section ring lasers based on quantum dot materials: theory and simulations," Opt. Express **26**, 19044–19058 (2018).
33. M. Homar, J. V. Moloney, and M. S. Miguel, "Travelling wave model of a multimode fabry-perot laser in free running and external cavity configurations," IEEE Journal of Quantum Electronics **32**, 553–566 (1996).
34. A. Gordon, C. Y. Wang, L. Diehl, F. X. Kärtner, A. Belyanin, D. Bour, S. Corzine, G. Höfler, H. C. Liu, H. Schneider, T. Maier, M. Troccoli, J. Faist, and F. Capasso, "Multimode regimes in quantum cascade lasers: From coherent instabilities to spatial hole burning," Physical Review A **77**, 053804 (2008).
35. J. Javaloyes and S. Balle, "Mode-locking in semiconductor fabry-pérot lasers," IEEE Journal of Quantum Electronics **46**, 1023–1030 (2010).
36. A. Pérez-Serrano, J. Javaloyes, and S. Balle, "Longitudinal mode multi-

stability in ring and fabry-pérot lasers: the effect of spatial hole burning," Optics Express **19**, 3284–3289 (2011).
37. M. Rossetti, P. Bardella, and I. Montrosset, "Time-domain travelling-wave model for quantum dot passively mode-locked lasers," IEEE Journal of Quantum Electronics **47**, 139–150 (2011).
38. J. Renaudier, G.-H. Duan, P. Landais, and P. Gallion, "Phase correlation and linewidth reduction of 40 GHz self-pulsation in distributed bragg reflector semiconductor lasers," IEEE Journal of Quantum Electronics **43**, 147–156 (2007).
39. J. Müller, J. Hauck, B. Shen, S. Romero-García, E. Islamova, S. S. Azadeh, S. Joshi, N. Chimot, A. Moscoso-Mártir, F. Merget, F. Lelarge, and J. Witzens, "Silicon photonics WDM transmitter with single section semiconductor mode-locked laser," Advanced Optical Technologies **4** (2015).